J. Fluid Mech. (1987), *vol.* 174, *pp.* 313–326
Printed in Great Britain

Convection in a rotating cylindrical annulus. Part 2. Transitions to asymmetric and vacillating flow

By A. C. OR
Department of Earth and Space Sciences, University of California, Los Angeles, USA

AND F. H. BUSSE
Institute of Geophysics and Planetary Physics, University of California, Los Angeles, USA
and University of Bayreuth, West Germany

(Received 19 November 1985 and in revised form 7 June 1986)

The instabilities of convection columns (also called thermal Rossby waves) in a cylindrical annulus rotating about its axis and heated from the outside are investigated as a function of the Prandtl number P and the Coriolis parameter η^*. When this latter parameter is sufficiently large, it is found that the primary solution observed at the onset of convection becomes unstable when the Rayleigh number exceeds its critical value by a relatively small amount. Transitions occur to columnar convection which is non-symmetric with respect to the mid-plane of the small-gap annular layer. Further transitions introduce convection flows that vacillate in time or tend to split the row of columns into an inner and an outer row of separately propagating waves. Of special interest is the regime of non-symmetric convection, which exhibits decreasing Nusselt number with increasing Rayleigh number, and the indication of a period doubling sequence associated with vacillating convection.

1. Introduction

Convection in the form of thermal Rossby waves is the typical flow that occurs in rotating fluids when the density is unstably stratified and the vectors of gravity and rotation do not coincide. Thermal Rossby waves have thus become of central interest to scientists working on the dynamics of planetary liquid cores or on convection in the deep atmospheres of the major planets. For a review of some recent work we refer to Busse (1982).

Thermal Rossby waves are also of interest by themselves as a unique phenomenon in fluid mechanics. They represent the onset of a convective instability in the form of a propagating wave. Because the direction of propagation is determined by the direction of rotation, the time dependence is quite different from other forms of oscillating convection. This difference manifests itself in the nonlinear properties. In an earlier paper (Busse & Or 1986; hereinafter referred to as I) we have shown that a mean zonal flow is generated by thermal Rossby waves. The time dependence and the growth of a mean zonal shear cause a saturation of the convective heat transport. In this paper it will be shown that both effects are amplified by a transition to a new form of convection. This secondary form of convection is characterized by decreasing heat transport with increasing Rayleigh number.

The analysis of this paper is restricted to two-dimensional convection, since three-dimensional modes are not possible until much higher Rayleigh numbers are reached than are considered in this paper (Busse 1970). The restriction to two

dimensions permits the analysis of the stability of the secondary form of convection and the study of finite-amplitude tertiary solutions. Of particular interest are the vacillating solutions found in this connection.

Section 2 gives an outline of the basic equations and the numerical Galerkin method used to solve them. As in I, the case of vanishing curvature of the conical axial boundaries of the annulus and the case of finite curvature will be considered separately. Most of the attention will be focused on the former case. Instabilities of the primary solution are discussed in §3, and secondary solutions and their stability explored in §4. Section 5 describes a few cases in which finite-amplitude tertiary solutions have been obtained. In §6 the stability problem of thermal Rossby waves in the presence of finite curvature is described. The paper closes with a discussion of possible relationships between the theoretical solutions and dynamical phenomena observed on the major planets.

2. Basic equations and method of solution

We consider motions introduced by centrifugal buoyancy in a cylindrical annulus of height L and thickness D with a mean radius r_0. The temperatures T_1 and T_2 ($T_2 > T_1$) are kept constant on the inner and outer walls, respectively. A dimensionless description of the problem is obtained by using D as the lengthscale, D^2/ν as the timescale where ν is the kinematic viscosity, and $(T_2 - T_1)\,P$ as the temperature scale. Since the small-gap approximation, $D \ll r_0$, is used, a Cartesian system of coordinates may be used with the x, y, z-coordinates pointing in the radial, azimuthal and axial directions, respectively. Stress-free conditions are satisfied by the velocity field on the cylindrical surfaces,

$$v_x = \frac{\partial^2}{\partial x^2} v_x = 0 \quad \text{at } x = \pm\tfrac{1}{2}. \tag{2.1}$$

The boundaries in the axial direction are of conical shape and are assumed to be symmetric with respect to the equatorial plane of the annulus

$$v_z + \eta_0(1+\epsilon x)\, v_x = 0 \quad \text{at } z = \pm\frac{1}{2}\frac{L}{D}, \tag{2.2}$$

where ϵ describes the radial curvature of these boundaries. The tangent η_0 of the mean angle of inclination with respect to the equatorial plane is considered to be a small parameter of the problem which allows us to describe the velocity as nearly geostrophic,

$$\boldsymbol{v} = \boldsymbol{\nabla} \times \boldsymbol{k}\psi(x, y, t) + \boldsymbol{\breve{v}}, \tag{2.3}$$

where $\boldsymbol{\breve{v}}$ is of the order η_0 smaller than the geostrophic part. As shown in I, the equation for ψ can be written in the form

$$\left(\frac{\partial}{\partial t} + \frac{\partial}{\partial y}\psi\frac{\partial}{\partial x} - \frac{\partial}{\partial x}\psi\frac{\partial}{\partial y}\right)\Delta_2\psi - \eta^*(1+\epsilon x)\frac{\partial}{\partial y}\psi - \Delta_2^2\psi + R\frac{\partial}{\partial y}\theta = 0, \tag{2.4a}$$

where Δ_2 denotes the two-dimensional Laplacian and θ is the deviation of the temperature from the conduction solution of the basic static state. The heat equation for θ assumes the form

$$P\left(\frac{\partial}{\partial t} + \frac{\partial}{\partial y}\psi\frac{\partial}{\partial x} - \frac{\partial}{\partial x}\psi\frac{\partial}{\partial y}\right)\theta + \frac{\partial}{\partial y}\psi - \Delta_2\theta = 0. \tag{2.4b}$$

The following dimensionless parameters have been introduced:

Rayleigh number $R \equiv \dfrac{\gamma D^3 \Omega^2 r_0 (T_2 - T_1)}{\nu\kappa}$,

Coriolis parameter $\eta^* \equiv \dfrac{4\eta_0 \Omega D^3}{\nu L}$,

Prandtl number $P = \dfrac{\nu}{\kappa}$,

where γ is the coefficient of thermal expansion, Ω is the rate of rotation and κ is the thermal diffusivity. The parameter η^* is a measure of the dynamic constraint of rotation. In analogy to the β-plane effect used in meteorology, the parameter η^* describes the effect of the stretching of vortex tubes as they change their distance from the axis of rotation. While η_0 is small, η^* will be assumed to be of the order one or larger in the present study.

For the numerical analysis of (2.4) we use the same Galerkin method as in I, i.e. we search for solutions of the form

$$\psi = \sum_{l,\,n} \sin l\pi(x+\tfrac{1}{2}) \{\hat{a}_{ln} \cos n\alpha(y-ct) + \check{a}_{ln} \sin n\alpha(y-ct)\} + \xi \sum_{l=\text{odd}} \hat{a}_{l0}\, l\pi(x^2-x), \quad (2.5a)$$

$$\theta = \sum_{l,\,n} \sin l\pi(x+\tfrac{1}{2}) \{\hat{b}_{ln} \cos n\alpha(y-ct) + \check{b}_{ln} \sin n\alpha(y-ct)\}. \quad (2.5b)$$

In contrast to I, the coefficients $\hat{a}_{ln}, \check{a}_{ln}, \hat{b}_{ln}, \check{b}_{ln}$ may be functions of the time t. The second sum in (2.5a) is added in order that the mean zonal flow component satisfies periodic boundary conditions across the layer for $\xi = 1$. For $\xi = 0$ the case of stress-free boundaries is obtained, which will be studied in a few cases; but unless otherwise specified $\xi = 1$ will be assumed. The case $\xi = 1$ can also be motivated by the application of the theory to a laboratory annulus with rigid boundary conditions. In that case stress-free boundary conditions can be justified for the fluctuating component of motion at least in the asymptotic case of high η^* because of the small azimuthal wavelength (Busse 1970). For the mean component of motion the rigid boundary conditions are satisfied for $\xi = 1$ if an appropriate constant velocity is added which will not affect the solution because of the Galilean invariance of the problem.

After inserting expansions (2.5) into (2.4), multiplying those equations by the expansion functions and averaging them over the domain $-\frac{1}{2} \leqslant x \leqslant \frac{1}{2}$, $-\infty < y < \infty$ we obtain a system of nonlinear equations for the unknowns $\hat{a}_{ln}, \check{a}_{ln}, \hat{b}_{ln}, \check{b}_{ln}$,

$$(1+\delta_{m0}) \left[\frac{\mathrm{d}}{\mathrm{d}t} + k^2\pi^2 + m^2\alpha^2\right] (k^2\pi^2 + m^2\alpha^2)\, \hat{\alpha}_{km} - m\alpha c (k^2\pi^2 + m^2\alpha^2)\, \check{\alpha}_{km} + \eta^* H_{kmln}\, \check{a}_{ln} - Rm\alpha \check{b}_{km} + I_{kmlnkp}\, \hat{a}_{ln}\, \check{a}_{kp} = 0, \quad (2.6a)$$

$$\left[\frac{\mathrm{d}}{\mathrm{d}t} + (k^2\pi^2 + m^2\alpha^2)\right] (k^2\pi^2 + m^2\alpha^2)\, \check{\alpha}_{lk} + m\alpha c (k^2\pi^2 + m^2\alpha^2)\, \hat{a}_{km} - \eta^* H_{kmln}\, \hat{a}_{ln} + Rm\alpha \hat{b}_{km} + \hat{I}_{kmlnkp}\, \hat{a}_{ln}\, \hat{a}_{kp} + \check{I}_{kmlnkp}\, \check{a}_{ln}\, \check{a}_{kp} = 0, \quad (2.6b)$$

$$(1+\delta_{m0}) \left[P\frac{\mathrm{d}}{\mathrm{d}t} + k^2\pi^2 + m^2\alpha^2\right] \hat{b}_{km} - Pm\alpha c \check{b}_{km} + \hat{J}_{kmlnkp}\, \hat{a}_{ln}\, \check{b}_{kp} + \check{J}_{kmlnkp}\, \check{a}_{ln}\, \hat{b}_{kp} = 0, \quad (2.6c)$$

$$\left[P\frac{\mathrm{d}}{\mathrm{d}t} + k^2\pi^2 + m^2\alpha^2\right] \check{b}_{km} + Pm\alpha c \hat{b}_{km} + \hat{L}_{kmlnkp}\, \hat{a}_{ln}\, \hat{b}_{kp} + \check{L}_{kmlnkp}\, \check{a}_{ln}\, \check{b}_{kp} = 0. \quad (2.6d)$$

The summation convention has been assumed in writing equations (2.6). The matrices $\boldsymbol{I}$, $\hat{\boldsymbol{I}}$, $\check{\boldsymbol{I}}$, $\boldsymbol{J}$, $\hat{\boldsymbol{J}}$, $\boldsymbol{L}$, $\hat{\boldsymbol{L}}$ and $\boldsymbol{H}$ represent lengthy expressions and will not be given here explicitly. Because of the translational invariance of the problem in the y-direction it is convenient to fix the phase of one of the terms in the representation (2.5a) with respect to the coordinate system drifting with the appropriate phase speed c. We arbitrarily set $\check{a}_{11}$ equal to zero and use (2.6b) with $k = 1$, $m = 1$ to determine c. R, α, P and η^* are regarded as prescribed parameters.

Three types of analysis have been performed on the basis of (2.5) and (2.6). First solutions with time-independent coefficients $\hat{a}_{ln}, \check{a}_{ln}, \hat{b}_{ln}, \check{b}_{ln}$ are obtained by a Newton–Raphson iteration. These solutions correspond to steadily drifting nonlinear Rossby waves and will be called stationary solutions. In a second step the stability of these solutions is analysed by superimposing infinitesimal disturbances,

$$\tilde{\psi} = \sum_{l,\,n} \sin l\pi(x+\tfrac{1}{2})\,\tilde{a}_{ln} \exp\{\mathrm{i}(n\alpha+d)(y-ct)+\sigma t\} + \xi(x^2-x) \sum_{l=\mathrm{odd}} l\pi\tilde{a}_{l0} \exp\{\mathrm{i}d(y-ct)+\sigma t\}, \quad (2.7a)$$

$$\tilde{\theta} = \sum_{l,\,n} \sin l\pi(x+\tfrac{1}{2})\,\tilde{b}_{ln} \exp\{\mathrm{i}(n\alpha+d)(y-ct)+\sigma t\}, \quad (2.7b)$$

on to the stationary solutions ψ, θ. The derivation of the equations for the unknowns $\tilde{a}_{ln}, \tilde{b}_{ln}$ is analogous to that of (2.6). The equations are linear and homogeneous and the time derivative is replaced by σ. The condition that the determinant of the coefficients of $\tilde{a}_{ln}, \tilde{b}_{ln}$ vanishes yields an equation for the eigenvalue σ. Whenever the real part σ_{r} of σ becomes positive as a function of the Floquet parameter d, the stationary solution ψ, θ is unstable. When all values σ_{r} are negative, the stationary solution can be considered to be stable, since expressions (2.7) represent the most general form of two-dimensional disturbances. Growing three-dimensional modes occur only at Rayleigh numbers which exceed the critical value R_{c} for two-dimensional ones by a factor of the order $(\eta^*)^{-\frac{4}{3}}$ according to the linear asymptotic analysis of I and earlier work mentioned there. Three-dimensional disturbances will thus be relevant only at much higher values of R than are of interest in the present study, provided η^* is sufficiently large.

When the stationary solution becomes unstable, a different stationary solution may bifurcate from it, or a more complicated time-dependent solution may replace it. Solutions of the latter type can be analysed by solving (2.6) for time-dependent coefficient $\hat{a}_{ln}(t)$, $\check{a}_{ln}(t)$, $\hat{b}_{ln}(t)$ and $\check{b}_{ln}(t)$. A semi-implicit Runge–Kutta scheme is employed for the forward integration in time of the equations. The vacillating solutions described in §5 are obtained in this way. It must be admitted, however, that this method of solution requires that the solution be periodic in y. By replacing α by an appropriate small rational fraction of it, periodicity intervals different from that of the unstable stationary solution can be accommodated. But because of computational expenses and problems of numerical convergence this possibility is of limited use.

For the actual computational realizations of the three types of analysis outlined above the systems of equations must be truncated. As in I, equations and coefficients $\hat{a}_{ln}$ etc. are neglected if the inequality,

$$l+n > N_{\mathrm{T}},$$

holds where N_{T} is a suitably chosen positive integer. For most of the computations of the present study $N_{\mathrm{T}} = 4$, $N_{\mathrm{T}} = 5$ or $N_{\mathrm{T}} = 6$ have been used. To test the

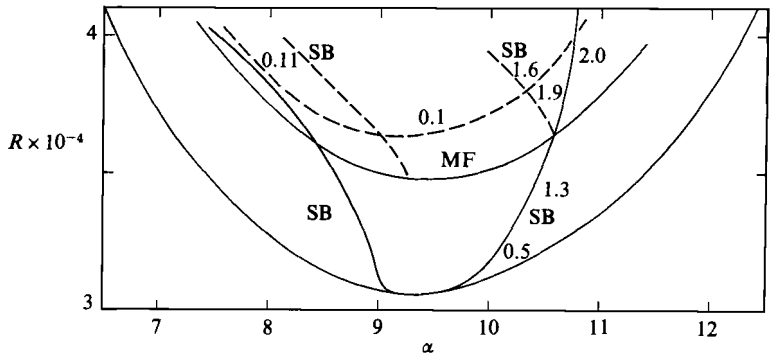

FIGURE 1. Stability boundaries (solid lines) of the primary solution for $P = 1$, $\epsilon = 0$, $\eta^* = 2800$. Solutions are stable within the region bounded by the side-band (SB) and mean-flow (MF) instabilities. The lowermost curve is the neutral curve for onset of convection. The dashed lines correspond to the stability boundaries of the secondary solution discussed in §4. The numbers refer to the values of d for the growing disturbances. $d = 0$ on curves without numbers.

convergence of the solutions, $N_T = 8$ has sometimes been used, especially for the primary solution and the analysis of its stability, since symmetry properties reduce the number of coefficients in this case. In general it has been found that the replacement of $N_T = 6$ by $N_T = 8$ causes insignificant changes in the solutions in the part of the parameter space that has been investigated. We shall return to the question of convergence at several points later in this paper.

3. Instabilities of symmetric thermal Rossby waves

It has been shown in I that for $\epsilon = 0$ the system of equations (2.6) admits a subclass of solutions for which all coefficients $\hat{a}_{ln}$, $\check{a}_{ln}$, $\hat{b}_{ln}$, $\check{b}_{ln}$ with $l+n =$ odd vanish. This subclass describes symmetric thermal Rossby waves and includes the solution which replaces the static state when the convection instability sets in. In this section the instabilities of symmetric thermal Rossby waves will be described.

Because of the symmetry of the stationary solution the solutions of the stability equations separate into two classes: the class of 'even' disturbances has vanishing coefficients $\tilde{a}_{ln}$, $\tilde{b}_{ln}$ whenever $l+n$ is odd, while the opposite is true for the class of 'odd' disturbances. A particularly interesting instability belongs to the latter class. It is called the mean-flow instability, since its interaction with the stationary solution gives rise to a strong mean zonal flow, as we shall discuss in more detail in the next section. This instability is characterized by the property that σ_r reaches is maximum value for $d = 0$. the instability thus does not exhibit the tendency to change the wavelength of the stationary solution. The mean-flow instability limits the region of symmetric thermal Rossby waves for Prandtl numbers of the order unity and for values of η^* of the order 10^3. A typical case is shown in figure 1 (the dashed lines in figures 1 and 2 should be ignored for the discussion of this section).

The parabolic stability boundary (SB) shown in figure 1 corresponds to a side-band instability, i.e. it is described by even disturbances which grow for small but finite values of d. Close to the critical point (R_c, α_c) the instability resembles in all respects the Eckhaus instability of ordinary Rayleigh–Bénard convection (Busse 1971, 1978). A difference develops, however, as the right branch of the stability boundary moves away from the critical point. The stability boundary no longer corresponds to vanishing d, but to finite values of d as indicated in the figure. The side-band

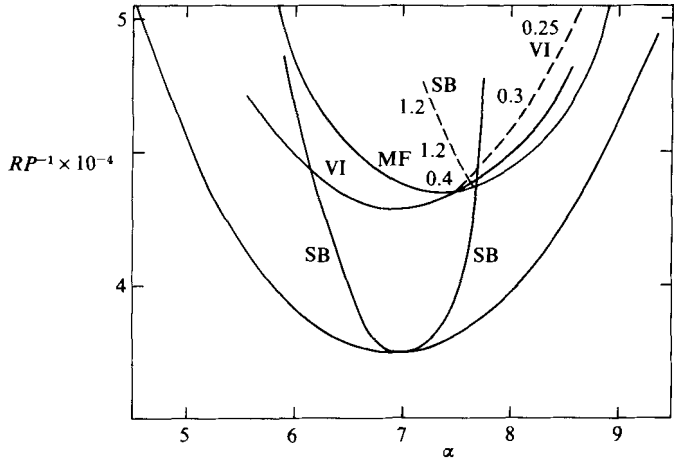

FIGURE 2. Same as figure 1 in the case $P = 0.3$. A new instability of the primary solution is the vacillation instability (VI), which occurs in modified form for the secondary solution as well.

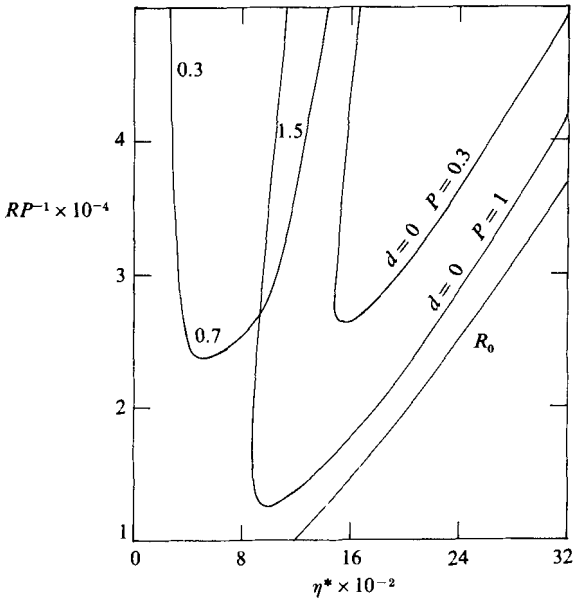

FIGURE 3. The variation of the mean-flow-instability boundary as a function of η^* for $P = 0.3$ and $P = 1$. The other parameters are $\epsilon = 0$, $\alpha = \alpha_c$. The neutral curve $R = R_0$ and another stability boundary in the upper left of the figure are shown for $P = 1$. The numbers along the latter curve refer to values of d.

instability limits the range of realizable wavenumbers α and has the tendency to shift the unstable solution towards $\alpha = \alpha_c$. According to the dispersion relation of linear thermal Rossby waves (see (2.10) of I), the frequency $\omega = \alpha c$ varies with α such that αc decreases when α increases and vice versa. As a consequence, growing side-band disturbances are associated with a positive value σ_i for positive d. This is easily understood since for $\alpha > \alpha_c$ the coefficient $\tilde{a}_{1-1}$ dominates in the side-band disturbance and the total frequency $\sigma_i + (\alpha - d)\, c$ is increased. For $\alpha < \alpha_c$ the coefficient $\tilde{a}_{11}$ dominates and the frequency $(\alpha + d)\, c - \sigma_i$ is decreased for positive σ_i.

For low Prandtl numbers another instability with growing odd disturbances appears and competes with the mean-flow instability. The new instability corresponds to a finite value of d as indicated in figure 2 and exhibits negative values of σ_i even in the limit of vanishing d. For reasons to be discussed in the next section we shall call this instability the vacillation instability. Because the growing disturbances are characterized by a small, but distinctly finite value of d, it is not possible to incorporate modes with the wavenumber $n\alpha+d$ for $n = 0, 1, \ldots$, into our numerical scheme without increasing the cost of computing enormously. It may be possible, however, to follow the nonlinear evolution of the disturbances by using asymptotic methods based on the property $d \ll \alpha$.

The dependence of the stability boundaries on η^* is indicated in figure 3. The graph confirms the expectation that convection rolls with the critical wavenumber α_c are stable with respect to two-dimensional disturbances in the limit of vanishing η^* which corresponds to the Rayleigh–Bénard case. There is still another instability not mentioned so far which limits the stability in the upper left-hand corner of the figure. Since this instability occurs in a region of the parameter space which is of lesser interest, it has not been studied in much detail. It corresponds to odd disturbances with a finite value of d. The mean-flow instability occurs at an approximately constant value of $R-R_c$ according to the figure, once a critical value of η^* has been exceeded. At values of η^* of the order 10^4 a new instability corresponding to a large positive value of σ_i precedes the mean-flow instability. This instability also corresponds to odd disturbances and exhibits a value of d which varies relatively little within the range $1.5 \lesssim d \lesssim 2.0$ for all values of η^* and P investigated in this paper. The maximum of the growth rate corresponding to this instability is even noticeable at lower values of η^* for $P \approx 0.3$. But in that region the instability is preceded by the vacillation instability, which corresponds to another maximum of the growth rate at lower values of d.

The majority of the stability computations have been done with $N_T = 6$ (7) for 'even' ('odd') disturbances. Eigenvalues σ have been computed on a grid in the (R, α)-plane and the actual position of the stability boundary has been determined by interpolation. Because of the smooth dependence of the eigenvalues σ on the parameters of the problem, the interpolation introduces a negligible error. By comparing the position of the stability boundary with results obtained for a higher truncation we estimate that the position is generally accurate within a few per cent of the supercritical Rayleigh number, $R-R_c$.

4. Secondary stationary solutions and their stability properties

Since the mean-flow instability corresponds to $d = 0$, $\sigma_i = 0$, it is relatively easy to follow the bifurcating solution. This solution differs from the primary symmetric solution in that the coefficients with odd $l+n$ no longer vanish. There are actually two secondary solutions; the second solution is obtained by reversing the sign of all coefficients $\hat{a}_{ln}$, $\check{a}_{ln}$, $\hat{b}_{ln}$, $\check{b}_{ln}$ with odd $l+n$. The two solutions are transformed into each other by reflection across the mid-plane of the layer. The introduction of coefficients with odd $l+n$ by the secondary solution is analogous to the effect of finite curvature on the primary solution. In both cases the convection eddies are shifted towards one or the other side of the layer, and strong Reynolds stresses are developed owing to the tilt of the eddies. Figure 4 shows the mean-flow profile for one of the two secondary solutions in the case of both stress-free and periodic boundary conditions. The graph for the other solution is obtained by replacing x by $-x$. The

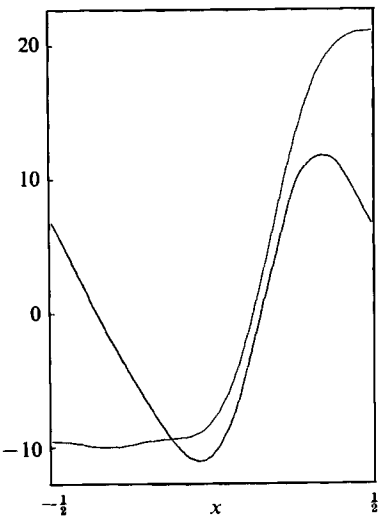

FIGURE 4. Profile of the mean zonal flow component of the secondary solution for stress-free and periodic boundary conditions. Parameters are $R = 7 \cdot 10^4$, $\epsilon = 0$, $P = 1$, $\alpha = 8$. The Nusselt number Nu and the drift rate are $Nu = 1.280$, $c = 16.227$ in the case of periodic boundary conditions and $Nu = 1.166$, $c = 22.27$ in the case of stress-free boundary conditions.

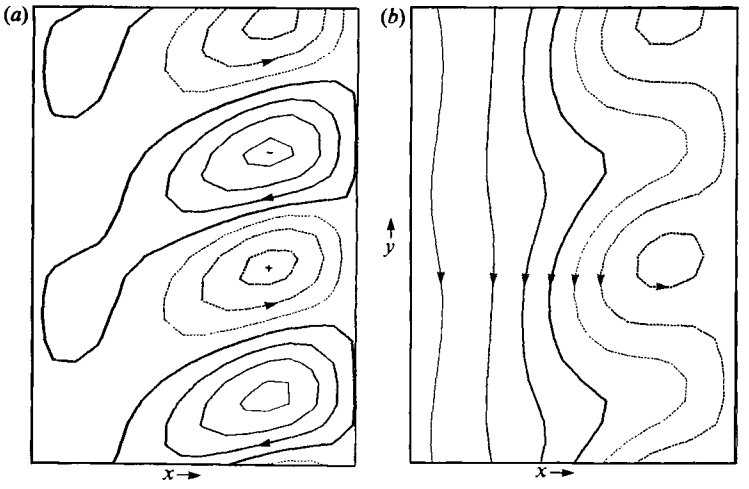

FIGURE 5. Steady streamline pattern of secondary solution as seen from the drifting frame of reference for $P = 1$, $R = 7 \cdot 10^4$, $\eta^* = 2800$, $\alpha = 8$, $\epsilon = 0$. (*a*) Shows streamlines without mean flow component, (*b*) includes mean-flow component.

streamlines of the secondary solution with and without the mean-flow component are shown in figure 5(*a*, *b*). Since the convection tends to be strongest where the mean zonal shear is strongest, only convective eddies with the same sign of vorticity as the vorticity of the zonal shear are visible when the shear is sufficiently strong.

That convection is especially strong on the side where the second derivative of the mean flow, $\partial^2 U/\partial x^2$, is negative can be understood in terms of a decrease of the constraint of rotation. As can be seen from (2.4*a*), the term $\partial^2 U/\partial x^2 \cdot \partial \psi/\partial y$ gives rise to a term of the same form but opposite sign as the term proportional to η^*, provided η^* is positive as has been assumed throughout this analysis.

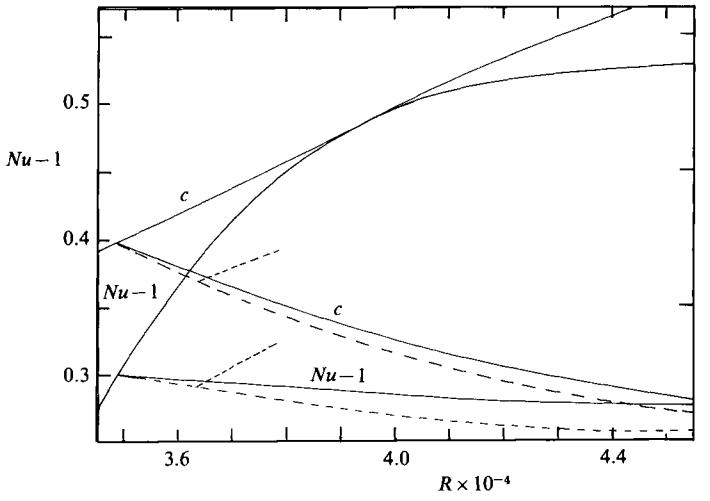

FIGURE 6. Nusselt number Nu and drift rate c of the secondary solution bifurcating from the corresponding curves of the primary solution. Also shown are c and the time average of $Nu-1$ for the tertiary solution in the form of vacillations which bifurcate from the secondary solution. The latter curves are given only for the truncation $N_T = 4$ (dashed lines). Parameters are $P = 1$, $\eta^* = 2800$, $\alpha = \alpha_c \approx 9.4$.

The tendency of the secondary solution to shift to one side of the layer has a dramatic effect on the convective heat transport.

Because the heat must be transported by conduction in the region where convection is weak, the shift of the convection eddies inhibits the heat flux. Figure 6 demonstrates that the heat flux actually decreases with increasing Rayleigh number as the secondary solution bifurcates from the primary one. Since the work done by the buoyancy force is proportional to the convective heat transport, the decrease of the heat transport leads to a concurrent decrease of the amplitude of convection.

Even though the curvature of the mean flow profile releases some of the rotational constraint, the secondary stationary solution does not appear to be very stable because of its inefficient heat transport. The stability analysis does indeed show that the domain of stability in the parameter space is relatively small. Figure 1 shows the stability region for $P = 1$. For lower values of P the region of stability rapidly decreases and at $P = 0.3$ there is only a minute region of stable secondary solutions left, as shown in figure 2. The main instability responsible for limiting the stability of the secondary solution is the vacillation instability. The name indicates the vacillation phenomenon that is introduced by the instability, as will be discussed below. The disturbances of maximum growth correspond to values of d of the order 0.1 nearly independent of η^*. The corresponding value of σ_i is about one third of αc for $\eta^* = 2800$ and varies little with d.

In addition to the vacillation instability there are the usual side-band mechanisms of instability. The corresponding boundaries are seen as dashed lines in figure 1 for $P = 1$, $\eta^* = 2800$. As in the case of the primary solution, the stability boundary on the left-hand side corresponds to disturbances with vanishing d, while on the right-hand side the critical disturbances have finite values of d. This difference is also noticeable in the discontinuities of the side-band stability boundaries at the onset of the secondary solution. While on the right-hand side only the slope changes discontinuously, on the left-hand side the stability boundary itself is shifted by a

finite amount. The latter feature can be understood in terms of the presence of the neutral displacement disturbance, $\tilde{\psi} = \partial\psi/\partial y$, $\tilde{\theta} = \partial\theta/\partial y$, from which the left side-band instability is derived as a perturbation.

The situation is more complicated at Prandtl numbers significantly larger than unity. For $P \gtrsim 2.5$ the maximum growth rate σ_r of the mean-flow instability is no longer obtained for vanishing d. Thus secondary solutions with the same azimuthal wavelength as the primary solution are not physically realistic. Instead, a modulated secondary solution must be expected, with d describing the wavenumber of the modulation. Since there are two secondary solutions, the modulation may be understood as a periodic sequence of one secondary solution alternating with the other. The mean-flow component of the secondary solution is changed into a large-scale circulation with the wavelength $2\pi/d$. This interpretation is supported by the fact that by far the largest disturbance coefficient in magnitude is $\tilde{a}_{10}$ in contrast to the side-band disturbances where $\tilde{a}_{1-1}$, $\tilde{a}_{11}$ dominate. Since eddies with relatively large scales in the azimuthal direction seem to predominate in the atmospheres of the major planets, the large-scale circulations are of particular interest. The study of their finite-amplitude properties requires a new numerical scheme, which permits the simultaneous representation of small- and large-scale eddies. The development of such a scheme will be a future project of the authors.

5. Tertiary solutions

It has not been possible to find stable tertiary stationary solutions which would replace the unstable secondary solutions. For this reason the more expensive approach for the solution of (2.6) by forward integration in time has been used. Since most instabilities correspond to finite values of d, it becomes cumbersome to follow the evolution in time of the corresponding growing disturbances. As has been mentioned before, the numerous modes that interact as the disturbance amplitude becomes finite cannot readily be represented in the numerical scheme that has been employed in this paper. Fortunately the growth rate of the vacillation instability in the case of the secondary solution changes very little from its maximum value when d approaches zero. It thus seems justified to restrict the attention to disturbances with $d = 0$, which can be analysed by including the same modes in the time integration scheme that have been used for the representation of the stationary secondary solution. In addition to its simplicity from the computational point of view, the choice of $d = 0$ can also be defended on the basis that only discrete values of d can be admitted in realistic situations when periodic conditions in the y-direction apply. Moreover, the value of d at which the growth rate reaches its maximum moves from 0.1 towards zero beyond the stability boundary in the case investigated here.

The finite value of σ_i at $d = 0$ indicates that the instability introduces a second frequency into the problem. The integration in time of (2.6) shows that the new time dependence assumes the form of a vacillation, i.e. the main effect is a periodic variation in time of the amplitude of convection. There is also a phase shift, however, between even and odd coefficients of the solution as indicated in figure 7. Thus a periodic 'breathing' occurs as the convection eddies shift their position with respect to the median plane of the layer. This 'breathing' may be responsible for the increase in the heat transport exhibited by the vacillating solution as shown in figure 7. By shifting eddies close to both boundaries in an alternating fashion the distance over which the heat is carried by conduction is kept small.

A particularly striking feature of the vacillation is the apparent period-doubling

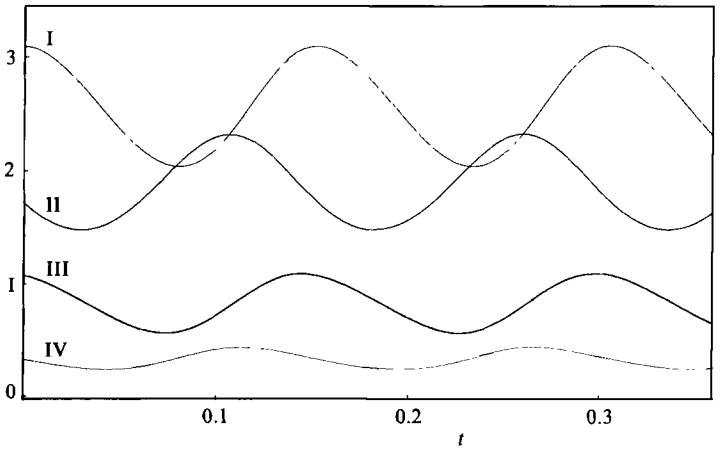

FIGURE 7. The time dependence of the functions $-\hat{a}_{10}$ (I), $(\hat{a}_{11}^2+\check{a}_{11}^2)^{\frac{1}{2}}$ (II), $(\hat{a}_{12}^2+\check{a}_{12}^2)^{\frac{1}{2}}$ (III), and $Nu-1$ (IV) in the case of the vacillating solution for $P=1$, $\eta^*=2800$, $R=3.8\cdot10^4$, $\alpha=9.4$, $N_T=5$. The period of vacillations is approximately six times the drift period $2\pi/\alpha c$ where $c=14.55$.

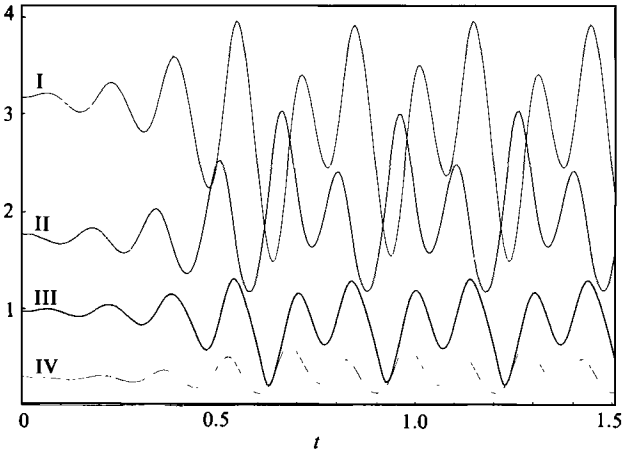

FIGURE 8. Transition from the unstable secondary solution to the vacillating solution with quadrupled period at $P=1$, $\eta^*=2800$, $R=3.9\cdot10^4$, $\alpha=9.4$, $N_T=5$. The roman numerals refer to the functions as in figure 7.

sequence. At $R=3.874\times10^4$ for $P=1$, $\eta^*=2800$, $\alpha=9.4$ a bifurcation to vacillations with twice the period of the original nearly sinusoidal vacillations takes place and a further bifurcation corresponding to a quadrupling of the period occurs at $R=3.899\cdot10^4$ (figure 8). It is likely that further period doublings do occur. But the demands for numerical accuracy and thus the costs of computations increase rapidly, and an alternative method of computation based on a Fourier analysis in time appears to be more suitable for the investigation of the period-doubling phenomenon. The solutions obtained at somewhat higher values of R exhibit slightly aperiodic behaviour and become increasingly chaotic as R is increased. While the Rayleigh number for the onset of the period-doubling sequence depends slightly on the truncation parameter, the phenomenon itself occurs in the same manner for all truncations that have been used. The above quoted values were obtained for $N_T=5$,

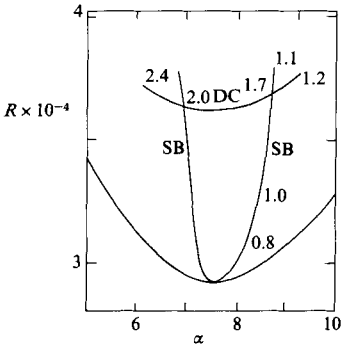

FIGURE 9. Stability boundaries of the primary solution in the case of finite curvature, $\epsilon = 1$ for $P = 1$, $\eta^* = 2800$. The region of stable columns is restricted by the onset of side-band instabilities (SB) and the double-column instability (DC). The numbers refer to values of d at the stability boundaries.

the corresponding values for the bifurcation points in the $N_T = 4$ approximation are lower by only about $0.028 \cdot 10^4$. Other kinds of truncation, as for example $l \leqslant 2$, $n \leqslant 4$, give similar results. We therefore conclude that the period-doubling phenomenon is an intrinsic property of the solutions which is not likely to disappear as N_T is increased.

6. Stability and transitions at finite curvature

In the case $\epsilon \neq 0$ even the basic solution exhibits asymmetries with respect to the median plane of the annular layer, as has been discussed in I. When ϵ becomes sufficiently large, the convection mode evolving from a double layer of convection columns in the limit $\epsilon = 0$ competes with the normal single-column-layer mode. When ϵ reaches 1 for $\eta^* = 2800$, the former solution dominates, and we shall focus attention on it. The stability diagram is shown in figure 9. The main difference in comparison with figure 1 is the narrowing of the stability region owing to the side-band instabilities. The stability region is limited towards high values of R by the onset of the double-column instability. While the primary solution exhibits convection columns which are nearly confined to the inner half of the annular layer, the growing disturbances of the double-column instability reach a maximum amplitude in the outer half of the layer. The growth rate reaches a maximum at the value of d indicated in figure 9 and the corresponding value of σ_i is around -40. These features together with a plot of the disturbance streamlines reveal that the instability tends to produce a second layer of convection columns which drift at their own rate in the outer half of the annular layer.

The tendency of the instability to form a second layer of convection columns has motivated us to seek solutions of a form in which two representations (2.5) are added, one with $\alpha = \alpha_1$, the other with $\alpha = \alpha_2 = \alpha_1 + d$. The only common terms in the representations are those with the coefficients $\hat{a}_{10}$ and $\hat{b}_{10}$. This mean-field approximation neglects all interactions between fluctuating terms which drift with different speed. The resulting form of convection streamlines without the mean flow component is shown in figure 10(*a*). As is evident from the forward inclination of the eddies towards the outside, the mean flow is prograde in the outer half of the layer and retrograde in the inner half.

The mean-field approximation introduced here should work well as long as the

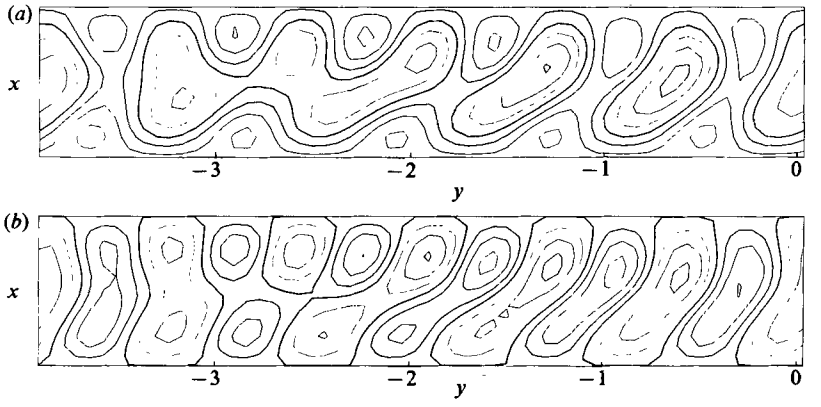

FIGURE 10. Instantaneous streamlines (*a*) with, and (*b*) without, mean-flow component in the case of the double-column solution (mean-field approximation). Parameter values are $R = 5 \cdot 10^4$, $\epsilon = 1$, $\eta^* = 2800$, $P = 1$, $Nu = 1.2751$, $\alpha_1 = 8$, $c_1 = 10.48$, $\alpha_2 = 9.6$, $c_2 = 16.71$.

neglected fluctuating interaction terms are small, since their linear effect on the solution vanishes in the time average. In future work it is planned to make a detailed comparison with more exact computations in order to assess the accuracy of the approximation.

7. Discussion

Because of the numerous external parameters of the problem only a small selection of the phenomena exhibited by thermal Rossby waves and their instabilities could be described. The large variety of instabilities is surprising since they are all restricted to two dimensions. In the case of Rayleigh–Bénard convection in a layer heated from below, two-dimensional instabilities of convection rolls are of minor importance and the stability boundaries are entirely determined by instabilities depending on the third spatial dimension. The time dependence of convection columns in a rotating annulus introduces new possibilities of interaction and thus causes the onset of the variety of new instabilities discussed in this paper. As a result of these instabilities convection in a rotating annulus attains a complex time dependence as soon as the Rayleigh number exceeds the critical value by a small fraction of the latter. This behaviour is also shown by experimental observations (Busse & Carrigan 1974; Azouni, Bolton & Busse 1986), which indicate persistence of the two-dimensional nature of the convection columns while their time dependence and azimuthal dependence become more complex as the Rayleigh number is increased. More sophisticated measuring techniques are needed in the laboratory experiments, however, before a quantitative comparison between experimental observations and theoretical predictions can be attempted.

The research reported in this paper has been motivated in part by the theory of convection in the deep atmospheres of Jupiter and Saturn (Busse 1976, 1983). The choices of values η^* used in the analysis are in part suggested by planetary applications for which values of η^* in the range 10^3 to 10^4 appear to be appropriate if an eddy viscosity of the order of 10^6 m^2/s is used (Busse 1983). The new results of the present paper indicate that the generation of mean zonal flows is a rather pervasive feature of convection in rotating annuli and spheres and that the finite curvature is not required for the generation of strong zonal flows. The sign of the

curvature parameter ϵ or any analogous parameter describing asymmetries of the annular layer will determine the direction of the mean zonal flow, however, and at $\epsilon = 1$ the primary solution exhibits a stronger growth of the mean zonal shear with increasing R than the secondary solution at $\epsilon = 0$. A surprising property of the secondary solution is the decrease of the amplitude of convection and the heat transport with increasing Rayleigh number, a feature which has also been observed in the experiment of Azouni *et al.* (1986). From the numerical work reported in §5 it appears that this trend can be counteracted by the onset of vacillating convection, at least for Prandtl numbers of order unity. It is of interest to note in this connection that vacillation phenomena have also been observed on Jupiter (Hatzes *et al.* 1981). The brown barges which seem to undergo oscillations are most likely centres of convective activity since they correspond to deeper regions in the atmospheres above which the cloud cover has been lifted. Among the other features observed on Jupiter which appear to be connected with convection in the deeper part of the atmosphere we mention the train of fairly regularly spaced plumes at the boundary of the north equatorial zone. The fact that the plumes trail behind the plume heads indicates that the latter propagate like waves in the prograde direction. This is what would be expected for thermal Rossby waves. The shape of the plumes resembles that which would be generated by the streamlines of figure 5(*b*) if the plumes emanated from the core of the cyclonic eddies. Obviously, the connection between the results of theoretical analysis and the observations on Jupiter is speculative at this point, and much more detailed models are required for a quantitative comparison with features observed on the major planets. The variety of solutions investigated in this paper indicates that several types of planetary eddies may be manifestations of columnar convection modes.

The research described in this paper has been supported by the Atmospheric Sciences Section of the US National Science Foundation.

REFERENCES

Azouni, M. A., Bolton, E. W. & Busse, F. H. 1986 Convection driven by centrifugal buoyancy in a rotating annulus. *Geophys. Astrophys. Fluid Dyn.* **34**, 301–317.

Busse, F. H. 1970 Thermal instabilities in rapidly rotating systems. *J. Fluid Mech.* **44**, 441–460.

Busse, F. H. 1971 Stability regions of cellular fluid flow. In *Instability of Continuous Systems* (ed. H. Leipholz), pp. 41–47. Springer.

Busse, F. H. 1976 A simple model of convection in the Jovian atmosphere. *Icarus* **20**, 255–260.

Busse, F. H. 1978 Nonlinear properties of convection. *Rep. Prog. Phys.* **41**, 1929–1967.

Busse, F. H. 1982 Thermal convection in rotating systems. In *Proc. 9th US Natl Congr. of Appl. Mech., ASME, New York*, pp. 299–305.

Busse, F. H. 1983 A model of mean zonal flow in the major planets. *Geophys. Astrophys. Fluid Dyn.* **23**, 153–174.

Busse, F. H. & Or, A. C. 1986 Convection in a rotating cylindrical annulus: thermal Rossby waves. *J. Fluid Mech.* **166**, 173–187.

Busse, F. H. & Carrigan, C. R. 1974 Convection induced by centrifugal buoyancy. *J. Fluid Mech.* **62**, 579–592.

Hatzes, A., Wenkert, D. D., Ingersoll, A. P. & Danielson, G. E. 1981 Oscillations and velocity structure of long-lived cyclonic spot. *J. Geophys. Res.* **86**, 8745–8749.